XX AIDAA Congress
Milano, Italy, June 29–July 3, 2009

STREAMWISE-TRAVELING WAVES OF SPANWISE WALL VELOCITY IN A PIPE FLOW: EXPERIMENTALLY ASSESSING THE TURBULENT DRAG REDUCTION

F.Auteri*, A.Baron*, M.Belan*, A.Bertolucci*, G.Gibertini* and M. Quadrio*

*Dipartimento di Ingegneria Aerospaziale
Politecnico di Milano, Campus Bovisa, Via La Masa 34, 20156 Milano, Italy
e-mail: maurizio.quadrio@polimi.it, web page:
http://www.aero.polimi.it/~quadrio

Keywords: Turbulent drag reduction, turbulent pipe flow

Abstract. *We report the first experimental assessment of the capabilities of an active, open-loop technique for drag reduction in turbulent wall flows that has been recently discovered (Quadrio* et al.*, J. Fluid Mech., 2009). The technique consists in generating waves of spanwise velocity that travel in the streamwise direction at the wall.*

A proof-of-principle experiment has been devised to assess drag reduction by the traveling waves. Although the available DNS data have been collected for the plane channel flow, in the present reserach we employ a circular pipe, where the sinusoidal spatial modulation of the azimuthal wall velocity is realized by subdividing an axial portion of the pipe into 60 thin slabs, which are driven by 6 independent shafts. Different speeds of nearby slabs provide, although in a discrete setting, the desired spatial variation of transversal wall velocity.

The drag is measured through the pressure drop across the active pipe length. Measurements are made particularly difficult by the tiny amount of pressure drop implied by the experimental conditions, that must be selected in order to obtain a large viscous length scale.

The results confirm the possibility of achieving large reductions of the friction drag in the turbulent regime. In our initial tests described in this paper, we have measured up to 26% drag reduction. The largest drag reductions are found for slowly forward-traveling waves, thus confirming the results of the available DNS study. The present results also show a substantial drop of drag reduction when the waves travel forward with a phase speed comparable to the convection speed of near-wall turbulent structures.

However, we are unable to reproduce the significant drag increase predicted by DNS for comparable conditions. The reasons for this apparent discrepancy are discussed in the paper.

1 INTRODUCTION

Controlling wall-bounded turbulent flows to the aim of reducing the wall-shear stress is an important and challenging topic in modern fluid mechanics. The book by Gad-el-Hak [3] gives a general treatment of the subject. Such a reduction of wall friction has enormous beneficial effects in a number of technological and industrial applications that involve the interaction of a turbulent flow with a solid surface. One direct consequence is for example that less fuel may be consumed in transport applications or for propelling gas and oil along pipelines. In particular, modern aerospace industry is interested in improving the aerodynamic efficiency of aircrafts. Potential benefits are both environmental (reduced pollution from air transportation) and economic (fuel saving). For aeronautical industries, according to Ref. [14], viscous drag is the most relevant part of the total drag of a civil airplane, and it is also the most likely to be reduced in the foreseeable future, by employing turbulence and separation control technologies. The U.S. Committee on Theoretical and Applied Mechanics [4] has recently stated that the fundamental understanding of the turbulence problem as well as the development of flow control technology are two out of the five research areas expected to be most influential to the enhancement of industry in the future. As an example, it has been estimated that reduction of skin friction drag by 10% could result in 10 billion dollars saving per year for the shipping industry.

Drag reduction techniques may be classified as active or passive, depending on whether or not an external input of energy is required to achieve the purpose. In the first class, a considerable interest has been devoted to modifying the turbulence by imposing a large-scale forcing along the spanwise direction, either by a wall motion or a body force (see [6] for a review and [13] for a more recent extensive list of works on the subject). One way of enforcing the near-wall motion is to generate *spanwise-traveling* waves in the very proximity of the wall. Relevant works in this field are the numerical investigations reported in Refs. [1], [2], [16] and the experimental study described in Ref. [5]. These efforts show that skin-friction reductions up to 40% may be obtained, at the expense of significant energy expenditure. Conceivable implementations to date are limited to body force in conductive fluids, or are supposed to act at the wall. The only experimental test available [5] reported an *estimate* of 7.5% drag reduction by a flexible sheet undergoing a spanwise traveling wave motion.

A new discovery in the field of spanwise forcing has been published recently by Quadrio, Ricco & Viotti [10] (hereinafter indicated by QRV09), and promises to yield a unified view of the entire class of spanwise forcing, where our understanding of the interaction between the external forcing and the natural turbulence can be improved. In their DNS study, Quadrio *et al.* have observed that waves of spanwise velocity applied at the wall of a turbulent channel flow and *traveling in the streamwise direction* are capable of altering the natural turbulent friction significantly. In particular, depending on the parameters that define the waves, drag can be either increased or decreased, and at low Re full relaminarization has been achieved. Large drag reductions are obtained at the expense of very limited expenditure in energy, thus resulting in a largely positive overall energy budget. The divergence-free condition at the wall is not violated by the forcing, which acts at large scale, and has been shown by QRV09 to yield large drag reductions over a wide range of scales. This paper presents the first experimental assessment of the performance of the streamwise-traveling waves in a turbulent pipe flow.

The streamwise-traveling waves considered by QRV09 are described by:

$$w_w(x,t) = A\sin\left(\kappa_x x - \omega t\right), \tag{1}$$

where w_w is the spanwise (z) component of the velocity vector at the wall, x is the streamwise coordinate and t is time, A is the oscillation amplitude, κ_x is the wave number in the streamwise

direction and $\omega = 2\pi/T$ is the oscillation frequency. One important parameter of the waves is their phase speed $c = \omega/\kappa_x$ in the spanwise direction. Such waves include and generalize the particular cases of the oscillating wall [6], where the wall forcing is spatially uniform:

$$w_w(t) = A \sin(\omega t),$$

and the stationary transverse waves [12], where the forcing presents the appealing characteristic of being stationary

$$w_w(x) = A \sin(\kappa_x x).$$

(We note here, in passing, that Quadrio & Luchini, building on the concept of these stationary waves, have recently patented [9] a new kind of riblets, the so-called sinusoidal riblets, that work passively and offer improved performances above those of conventional riblets. In the meanwhile, independent observations [7], based on a numerical study, have been put forward to witness the potential of this approach.)

The effects exerted by the streamwise-traveling waves on the turbulent plane channel flow, as described by QRV09, are summarized in figure 1, that is adapted from that paper. The flow has a Reynolds number of $Re = 3170$ based on the bulk velocity U_b and the channel half-width h. The amplitude A of the waves is kept fixed at $A = 0.75U_b$. The figure reports the effect of waves as a function of their spatial and temporal frequency. Only half of the $\kappa_x - \omega$ plane is plotted, thanks to the simmetry of the results w.r.t. the origin of the plane. The effects of the waves change significantly in nature when moving on the $\kappa_x - \omega$ plane. The largest drag reduction (about 48% for this value of A) is observed for slowly forward-traveling waves over a wide range of not-too-large wavelenghts. At smaller κ_x, the maximum drag reduction pertains to backward-traveling waves when the wavelength $\lambda = 2\pi/\kappa_x$ of the waves exceeds $\lambda \approx 6h$. At a relatively well-defined phase speed c (indicated in this plot by the inverse of the slope of straight lines passing through the origin), the effect of the waves abruptly becomes that of drag increase. The straight line with $c = 0.7U_b$ identifies the locus of maximum drag increase. The effects of the forcing amplitude A and of the value of the Reynolds number have been partially addressed in Ref. [10]: DR increases with A and saturates at large amplitudes, whereas its reduction with increasing Re is within the known performances of related techniques, like the oscillating wall, and should not be critical owing to the hypothesized wall scaling. Quadrio in Ref. [8] gives the latest update on the process of understanding the mechanism, only hinted at in Ref. [10], by which the waves are capable of modifying friction drag, and points to the action of the transversal oscillating generalized (laminar) Stokes layer as the main responsible for this effect.

Aim of the present work is to give the results published by QRV09 an experimental confirmation. We use a circular pipe, since the cylindrical geometry allows for an easier implementation of the traveling waves, owing to the naturally periodic spanwise (azimuthal) direction. We will show that large rates of friction drag reduction are experimentally confirmed, though at the present stage of the research some experimental uncertainty is still blurring the picture concerning the exact scaling of DR and whether or not the results are affected by the particular (planar or cylindrical) geometry.

The present paper is organized as follows. In §2 the experimental setup is described, together with the required steps that we had to take in order to reliably measure friction drag. §2.1 describes the experimental conditions and procedures. §3 reports the main results, and a concluding discussion can be found in §4.

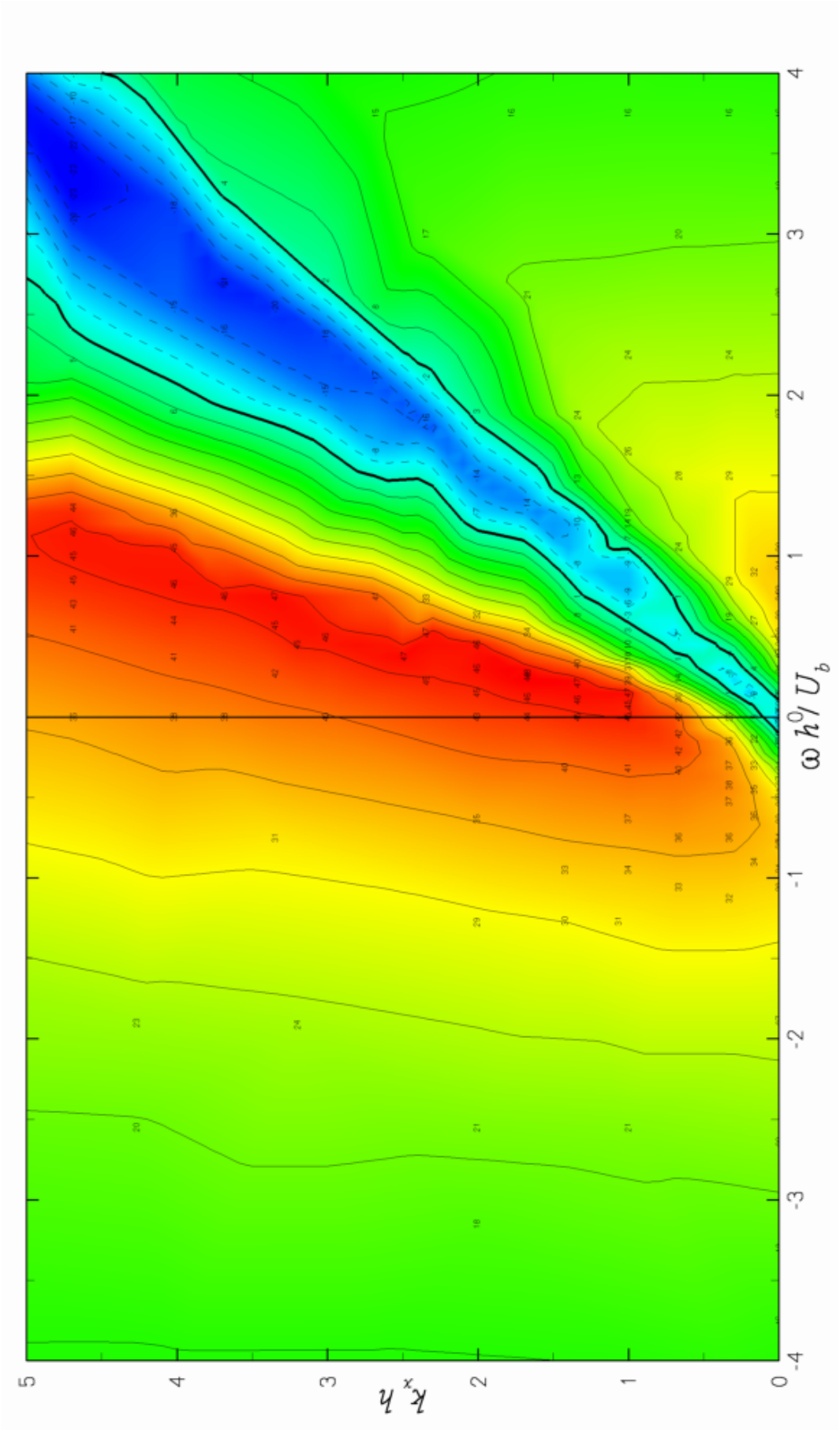

Figure 1: Map of friction drag reduction (percentage) in the $\omega - \kappa_x$ plane for $A = 0.75U_b$ and $Re = 3170$. Contours are spaced by 5% intervals, loci of zero DR are indicated by thick lines and negative values are represented by dashed lines. The numbers indicate percentage drag reduction at measured points. The range explored by the present experiment in the circular pipe is described later by the thick dashed lines in fig. 7.

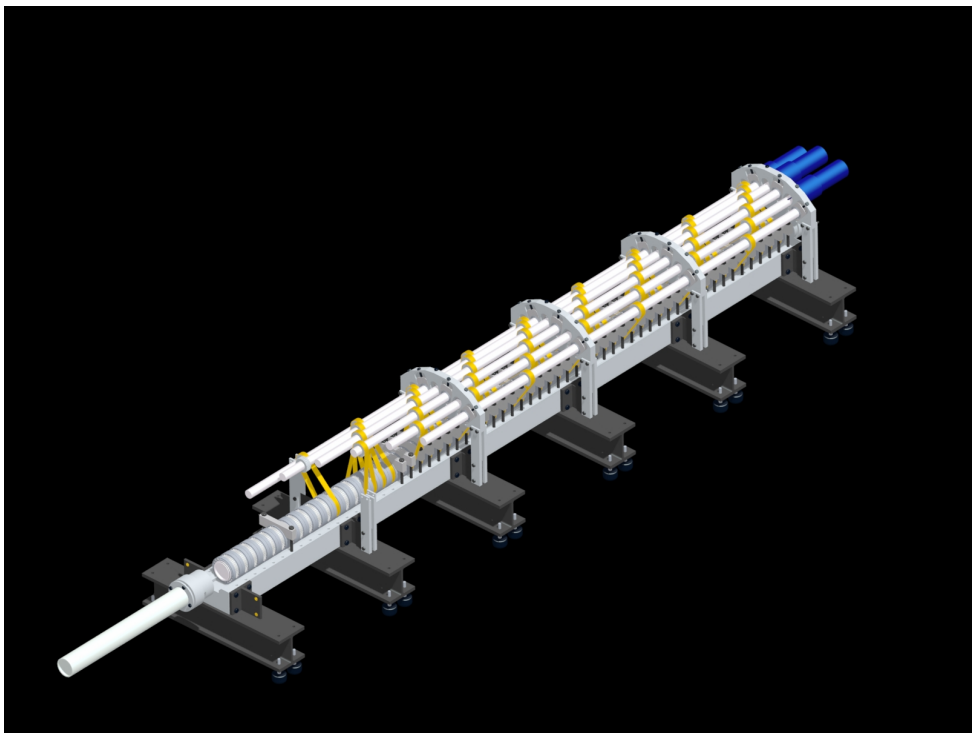

Figure 2: Drawing of the experimental setup. The oscillating slabs are supported by a steel rail. The active portion of the pipe is 2.2m long. The image shows the six transmission shafts, together with 3 of of 6 D.C. motors (top right). The remaining 3 motors (not shown) are installed on the opposite end of the shafts. The return pipe can be seen on the bottom left.

2 THE EXPERIMENTAL SETUP

The actual realization of the traveling waves is obviously not trivial, even for a proof-of-principle experiment like the present one. The traveling waves are described by Eq.(1), that prescribes a space-time distribution of spanwise (azimuthal) velocity at the wall. This can be implemented through a suitable spanwise blowing over a conventional wall, or – as in the present approach – thanks to a moving wall. It is thus the wall speed that enforces the control velocity required to generate the waves.

The temporal variation implied by Eq.(1) is directly enforced through a time-varying wall speed. The cylindrical geometry avoids difficulties in providing a uniform speed along the spanwise (azimuthal) direction. The sinusoidal variation along the streamwise direction, on the other hand, needs to be suitably discretized. In our setup, this is achieved by imposing different rotation rates to different longitudinal slabs of the pipe.

In addition to the traveling waves, the setup can be used to obtain both purely temporal oscillations, when all the pipe sections have an in-phase alternating motion, and purely spatial oscillations, when all the pipe sections steadily rotate at different speeds.

The longitudinal sinusoidal variation of the transversal velocity required by (1) is discretized through up to 6 independent pipe segments for each wavelength. Each segment has an axial length of 36.55 mm and an inner diameter of 50 mm. The total length of the pipe section with rotating segments is about 2.2 m, that amounts to no less than 10 wavelengths. The lineup of the different segments is achieved by mounting each segment with two rolling-contact bearings co-axial to the pipe and aligned to a steel rail. The need for controlling the frequency of the sinusoidal variation of the angular speed, and in particular for implementing a constant-speed motion, poses a number of constraints on the transmission system, that is based on timing belts

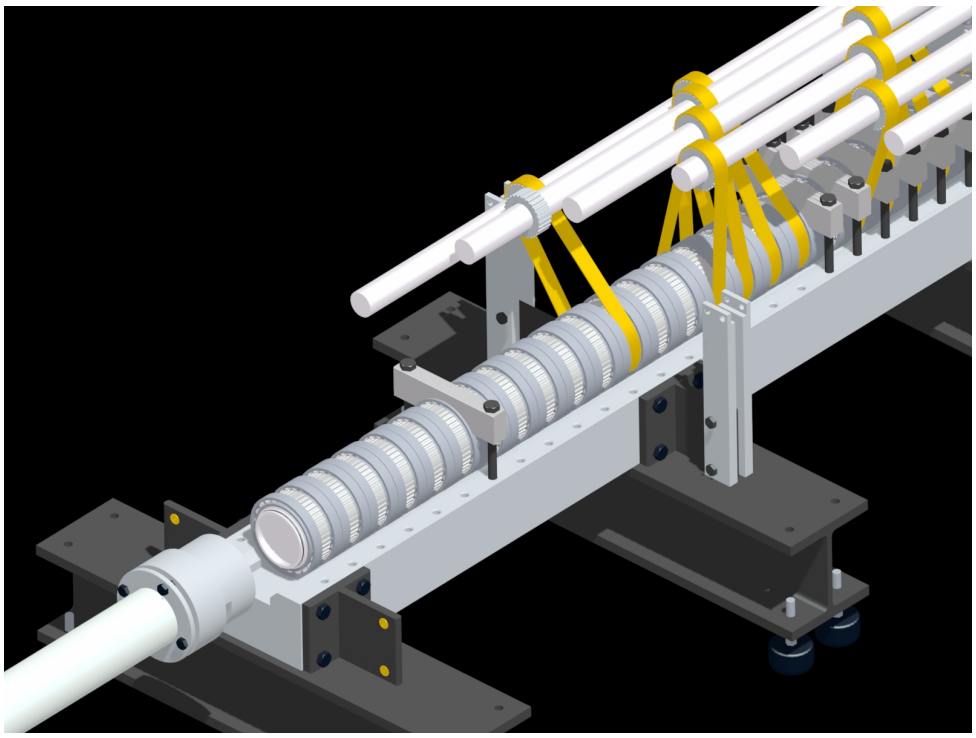

Figure 3: Close-up of the drawing of the trasmission system: detail of the shafts, belts and rotating segments, lined on the steel rail.

moved by 6 independent D.C. motors, each one driven by a purposely designed closed-loop controller. The portion of the pipe with rotating segments is part of a large closed-circuit pipe. The whole apparatus is approximately 250 diameters long, thus ensuring a fully developed turbulent flow, whereas the active part is 44 diameters long.

Particular care has been devoted to prevent water from leaking through the joints between the segments, or air from being sucked into the circuit. For this purpose, o-rings have been employed and a water-proof grease has been adopted to improve sealing and lubrication. To prevent grease from being sucked in the test section through the joints between the segments, absolute pressure in the test section has been adjusted through a closed-loop control system, that changed runtime the elevation of a moving reservoir to maintain a slight overpressure within the test section with respect to ambient.

Fig.2 reports a global view of a schematic of the experimental setup; a detailed view of the transmission system can be observed in fig.3. Lastly, fig.4 is a picture of a closeup of the transmission system.

The flow-rate, and hence the bulk velocity in the active section, is measured by means of an orifice plate device designed according to the international standard ISO 5167 and positioned in the return circuit. Honeycombs have been positioned in the circuit to avoid swirl. The flow meter was calibrated against a traceable standard instrument to improve accuracy.

Drag is evaluated by measuring the pressure drop between two points located immediately upstream the first rotating segment and immediately downstream the last one. The main source of error in the measurement chain is due to capillary effects in the pressure measurement tubing. In fact, to avoid sensor filling, a water-air separation surface is always present where capillary effects associated to contact angle uncertainty [15] produce an error in the pressure measurement which is inversely proportional to the tube diameter. To reduce the impact of such uncertainty, high diameter vessels, 20 mm for the flow measurent transducer tubing and 50 mm

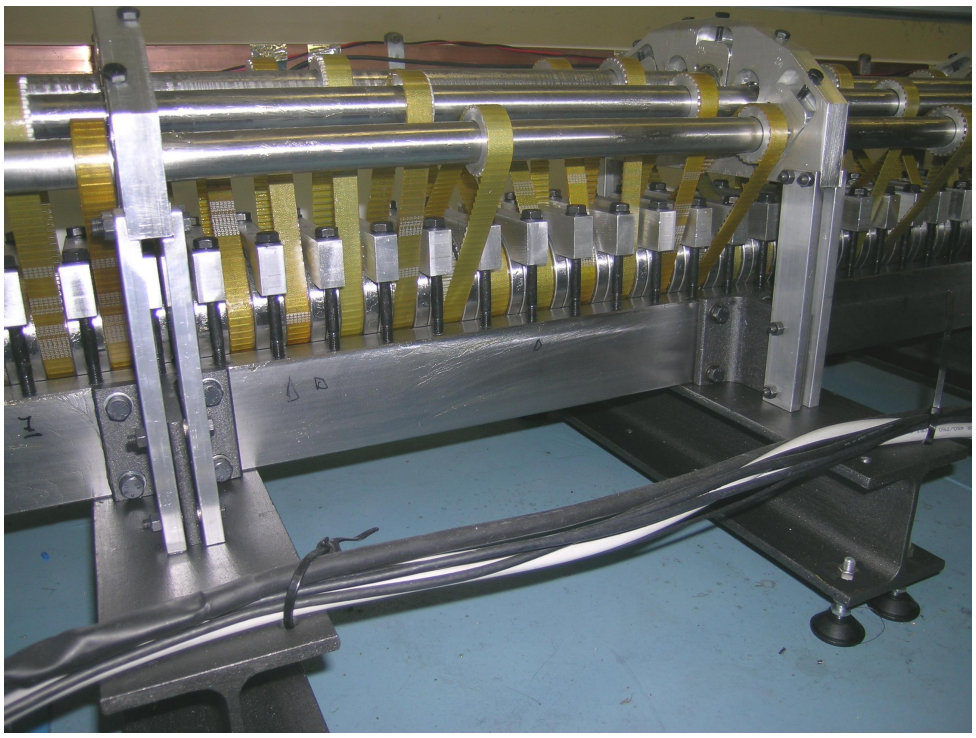

Figure 4: Picture of the experimental setup, showing a particular of the shafts, belts and moving segments. The segments are forced to line on the steel rail by suitable saddles.

for the head loss transducer, have been employed resulting in a ± 1 Pa ($\pm 0.1\%$) and ± 0.25 Pa ($\pm 2.5\%$) repeatability respectively.

The block diagram of the measurement system is reported in Fig.5. It is composed by a National Instruments PXI-1010 chassis optically connected to the test control computer. All signals have been digitized by a 18 bit high-accuracy multifunction acquisition (DAQ) module, PXI-6284. Reference signals for the motor controllers have been generated by a 16-bit analog output module, PXI-6733, which controlled also the pump inverter. The motor controllers are double closed-loop power amplifiers capable of 100W output power at $44V_{pp}$, where a tachymetric dynamo on each motor gives a signal used in a first analog loop inside the controller and, after A/D conversion, in a second digital loop through the PXI system.

Three pressure transducers were employed, a $0 \div 20$ mbar fullscale GE-Druck LPM 9481 for the flow-rate measurement, a $-2 \div 2$ mbar fullscale GE-Druck LPM 9481 for the head loss measurement and a $\pm 5''$ WC fullscale Setra for the pressure difference between the test section and the laboratory. A PT100 transducer has been employed to measure water temperature. Two solenoid valves driven by a PXI-2567 Relay module have been employed to zero the pressure transducers at the beginning of each measurement run.

2.1 Experimental conditions and procedures

Water is chosen as the working fluid. The bulk velocity of the flow is $U_b = 0.0895$ m/s and the value of the Reynolds number equals $Re = 4900$ (based on pipe inner diameter of 50 mm, water viscosity at the measured test temperature and U_b). In terms of friction Reynolds number, or Karman number R^+ in the turbulent pipe flow, this corresponds to $R^+ \approx 180$ and thus it is very near to the value of friction velocity based Reynolds number Re_τ employed in the DNS for the planar case. The R^+ is large enough for the flow to be fully turbulent, and

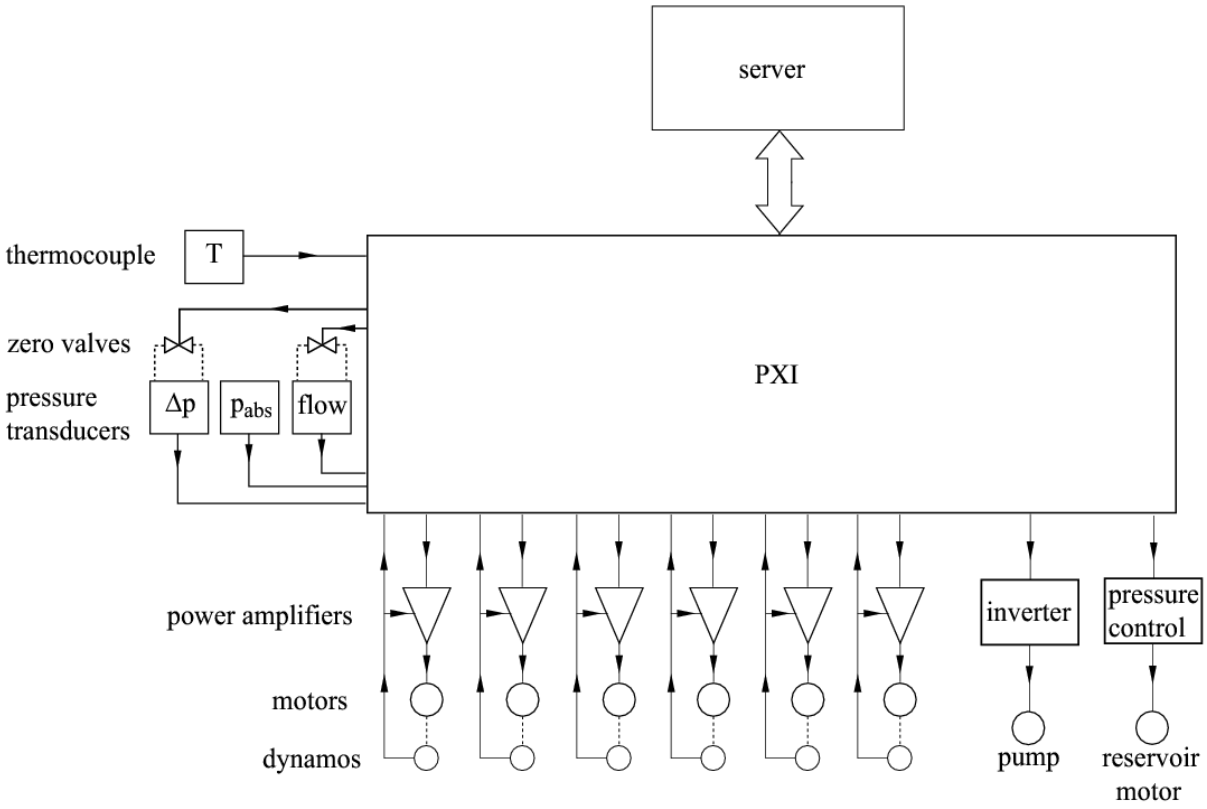

Figure 5: Block diagram of the measurement system. The pressure transducers are labelled as follows: Δp gives the value of the head loss across the active length of the pipe, with automatic zeroing, p_{abs} gives the test section absolute pressure and 'flow' gives the flow meter head loss, with automatic zeroing.

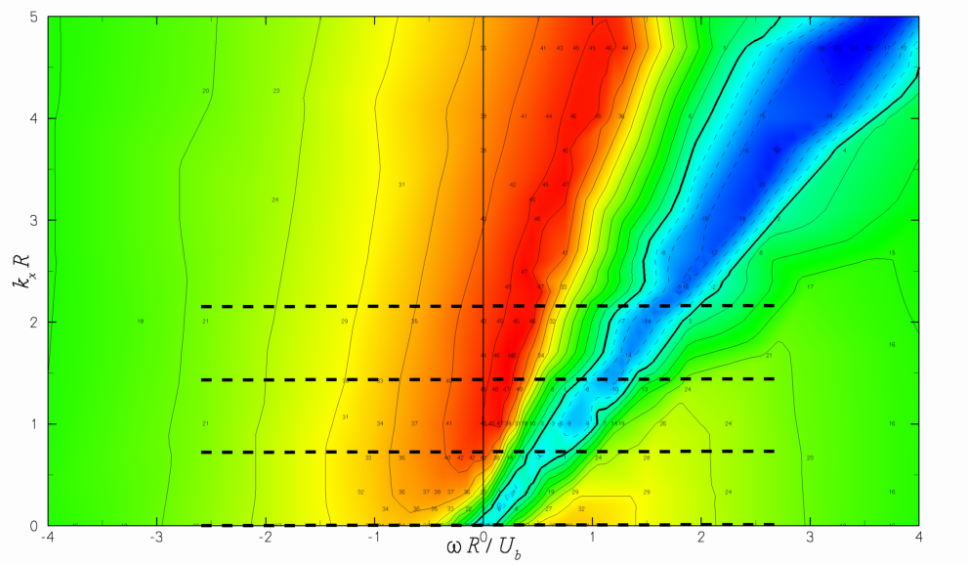

Figure 6: Range of waves parameters that can be explored with the present experimental setup, indicated by the dashed lines. The bottom dashed line corresponds to pure temporal oscillation of the pipe.

at the same time low enough to keep dimensions and frequencies of the drag-reducing device still manageable. In fact, the oscillating frequencies of interest are of the order of 1 Hertz; the pressure drop across the moving section is small but still measurable, of the order of 10 Pa.

Figure 6 shows the drag reduction map computed by DNS for the planar geometry, adapted from QRV09; the superimposed dashed lines serve the purpose of visualizing the parameter range that can be explored by the present experiment. The wall forcing can vary its wavelength from a minimum of two pipe segments, i.e. $\kappa_x R = 2.15$, to infinity, i.e. $\kappa_x = 0$. This last condition corresponds to a temporal wall oscillation which is uniform in space. Of course this variation of wavelength is severely quantized, as the number of motors limits to six the maximum number of segments that can be moved independently in one spatial period; the four discrete levels are thus $\kappa_x R = 0$, $\kappa_x R = 0.72$, $\kappa_x R = 1.43$ and $\kappa_x R = 2.15$. The temporal frequency can be varied continuously; its maximum value is limited by the mechanical and inertia characteristics of the device, by the transmission system and of course by the motors. The system has been designed so that at the maximum value of κ_x the available frequency is enough to observe the drag-increasing regime. The current limit of maximum frequency, shown in Fig.6 by the extrema of the dashed lines, corresponds to 1.5 Hz and is still below the mechanical limits of the actuation system.

The system, once filled with tap water, is left running to degas for a few hours. Bubbles are collected at the point with largest elevation in the circuit and left out. After visual inspection has confirmed that the flow is free of air bubbles, the actual measurements are taken. To minimize the effect of pressure fluctuations and electro-magnetic distrubances, quite long settling and acquisition times have been employed, namely 30 and 60 seconds respectively for one single point. An entire run of measurements is fully automated, and consists in about 200 points and thus takes a few hours of run time. For every experimental point, temperature is measured and the flow rate is adjusted to get the correct flow rate and Re_b before the pipe slabs are set into motion. After 30 seconds of settling time, the pressure signal is recorded for 40 seconds at an acquisition frequency of 1 kHz.

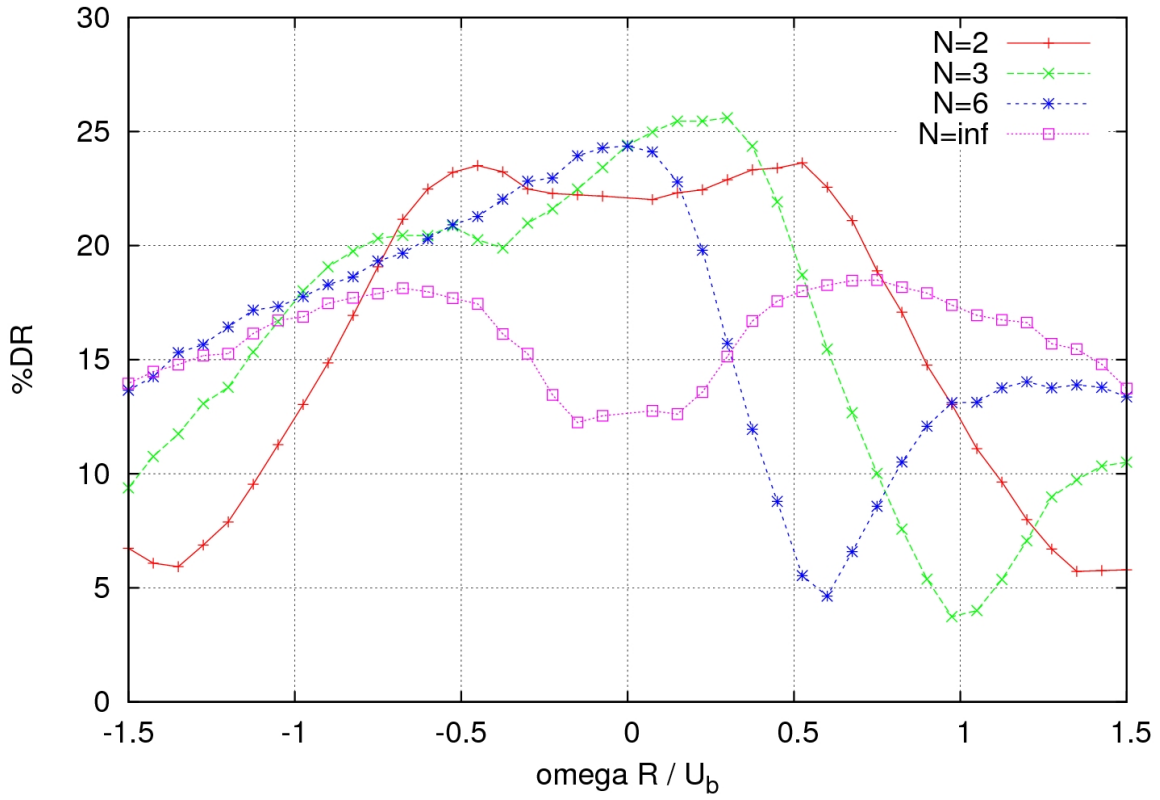

Figure 7: Friction drag reduction (in percentage of the reference friction) due to waves with $A = 0.62U_b$, as a function of the oscillation frequency.

3 RESULTS

A preliminary set of results is shown in figure 7. Percentage changes in friction drag are plotted against the oscillation frequency; the oscillation amplitude is kept fixed at $A = 0.62U_b$. This has to be compared with DNS results obtained for the plane channel flow at $A = 0.75U_b$. Judging from the preliminary study presented by QRV09 concerning the effects of amplitude A, the present value of A should yield values of drag reduction underestimated by 5-10% w.r.t the plane channel data.

The number N of segments that discretizes the spatial sinusoid and thus determines κ_x is also indicated in fig.7. The curve with $N = 0$ correponds to pure temporal oscillation, whereas $N = 6$ refers to the wave with the largest wavelength and the best spatial discretization of the sinusoid. It should be noted, in passing, that we believe the issue of the discretization of the spatial sinusoid through a number of segments as low as two to be not particularly critical. This follows from previous numerical studies, where the oscillating wall was tested in the planar geometry with the temporal waveform approximated by a simple square wave. No significant difference in the results has been reported.

The temporal frequency of the wave is varied in small steps, and the curves in fig.7 show how the turbulent friction changes along the points indicated by the dashed lines in fig.6.

The results indeed show most of the trends that one would expect based on the available DNS information for the planar geometry. Large drag reductions are succesfully measured, in particular at this forcing intensity we observe up to 26%. The maximum DR is observed at a wave frequency that depends on the wavenumber. The friction drag is reduced over the entire

range of parameters tested.

By looking at the results in more detail, one observes first that the curve for the temporally oscillating pipe is, as expected, symmetric between positive and negative frequencies. It presents the maximum DR at a frequency that confirms what is known [11] from previous (DNS) oscillating pipe results, i.e. corresponding to an optimal oscillation period near to 100 viscous time units.

The curve with $N = 2$ is symmetric between positive and negative frequencies, and this is a quite unexpected result. It can be seen clearly from fig.1 that data in the $\kappa_x - \omega$ plane are not symmetric for $\kappa_x > 0$, reflecting an important physical difference between forward- and backward-traveling waves. The reason for the symmetry in the measured data lies in the fact that the sinusoidal wave is discretized with only two segments; as a consequence, the speed of any two neighbouring segments is always in opposite direction. The wave is then basically a standing wave of the type

$$w_w(x,t) = A \sin(\kappa_x x) \sin(\omega t),$$

with no phase speed, which is the sum of two identical waves traveling in opposite directions with the same speed. It is interesting, however, to observe how the results are consistent with those for the forward-traveling wave. How the turbulent system selects the forward wave instead of the backward one is something that at present is still unclear.

Waves discretized with $N = 3$ and $N = 6$ do not suffer from such aliasing effect, and their behaviour is similar to what is expected. The frequency at which the maximum DR takes place is strongly wavelength-dependent; the optimal phase speed of the waves goes from a negative one (backward-traveling waves) for very large wavelengths to small and positive for shorter wavelengths. Indeed for $N = 6$ the maximum DR is observed for stationary or perhaps slowly-backward traveling waves, whereas when the wavelength is halved at $N = 3$ the optimum is clearly for forward-traveling waves with the relatively slow speed of $c = 0.35U_b$.

All the three curves corresponding to a spatially-nonuniform forcing clearly present a region, for positive frequencies and thus forward-traveling waves, where DR strongly diminishes. We are however unable to observe the actual increase of drag above the unperturbed level reported by QRV09. This local minimum in DR is, as expected, observed at a nearly constant value of the wave phase speed, namely $c = 1.2U_b$.

It must be said that, the general agreement notwithstanding, significant discrepancies exist between the present measurements and the available DNS dataset collected for the plane channel. As an example, the actual amount of maximum drag reduction turns out to be severely underestimated, by approximately 50%. More than one reason can explain this discrepancy, that will be discussed in the next Section.

4 DISCUSSION AND CONCLUSIONS

The experimental setup described here has been successfully used to generate streamwise-traveling waves of spanwise velocity at the wall of a pipe to modify the friction drag of a turbulent pipe flow. The capability of the waves to yield large reductions of drag has been clearly demonstrated in the laboratory, thus corroborating the numerical data available to date. The maximum observed drag reduction for the preliminary set of parameters tested here is in excess of 26%. The general dependence of the friction coefficient on the wave parameters is in good agreement with the available DNS information, that predicts the maximum DR for slowly forward traveling waves, and a local minimum for waves that travel with a phase speed which is comparable to the convection speed of the near-wall turbulent structures.

However, from a quantitative viewpoint several observations from our experimental campaign do not exactly correspond to the DNS data. For example, for the parameters mentioned above, DNS simulations reported by QRV09 yield a maximum DR of 45%, and – more strikingly – when the wave speed matches the turbulence convection velocity, DNS predicts a drag increase of 20% whereas we measure here a modest drag decrease (3%). Several arguments are relevant to explain this discrepancy.

First of all, the main mechanism suggested [8] to drive the modification of turbulent friction drag in plane channel flow is qualitatively different from what happens in the cylindrical geometry. This is something we are working on, but we can anticipate that the transversal oscillating layer (called Generalized Stokes Layer in Ref.[8]) acquires a wall-normal (radial) velocity component in the pipe geometry.

Moreover, our experimental setup differs in some respects from the idealized setting of a DNS. Most important is the presence of a spatial transient, where the turbulent friction gradually decreases from the unperturbed level. Our estimate, based on the DNS in cartesian geometry, is that this transient region extends over thousands of wall units, but this estimate applies to DR only. However, the pressure drop measured in the experiment is an integral measure over the entire active length of the pipe, and as such it yields an underestimated drag reduction / increase.

Last, and probably most important, the friction factor for the active pipe when the segments are held fixed is significantly higher than expected, by about 70%. This may be due to localized roughness effects, related either to the design of the pipe segments, or to debris or grease that accumulate in the measuring section. We are still working to sort out the reason for this macroscopical problem. At this stage, it is interesting to put forward the following observation. If one assumes the 70% overestimate in friction coefficient to be related to physical processes that cannot be affected by the drag-reduction capabilities of the waves, then the measured 26% reduction of the friction coefficient translates into a 45% reduction of that part of the pressure drop that can directly be associated with the distributed turbulent friction.

In conclusion, further work is definitely needed to sort out this issue. At the present stage, however, several significant results have been already achieved. Of capital importance is that our experimental setup has been successful for giving the large drag reduction due to the traveling waves an experimental confirmation. The 26% of drag reduction measured here, although preliminary, is one of the largest reductions of the turbulent drag ever obtained in the laboratory via modification of the flow boundary conditions. Moreover, we are confident to increase further this figure in the near future.

It is hoped that the capability of the traveling waves to affect the turbulent friction significantly will help shedding light on the mechanism by which wall turbulence is sensitive to spanwise forcing. This is an essential step towards exploiting such forcing to achieve turbulent drag reduction in real world applications.

REFERENCES

[1] Y. Du and G. E. Karniadakis. Suppressing Wall Turbulence by Means of a Transverse Traveling Wave. *Science*, 288:1230–1234, 2000.

[2] Y. Du, V. Symeonidis, and G. E. Karniadakis. Drag reduction in wall-bounded turbulence via a transverse travelling wave. *J. Fluid Mech.*, 457:1–34, 2002.

[3] M. Gad-el Hak. *Flow Control – Passive, Active and Reactive Flow Management*. Cambridge University Press, 2000.

[4] J. Gollub, H. Fernando, M. Garib, J. Kim, S. Pope, A. Smits, and H. Stone. Research in Fluid Dynamics: Meeting National Needs. Report of the U.S. National Committee on Theoretical and Applied Mechanics, 2006.

[5] M. Itoh, S. Tamano, K. Yokota, and S. Taniguchi. Drag reduction in a turbulent boundary layer on a flexible sheet undergoing a spanwise traveling wave motion. *J. Turbulence*, 7(27):1–17, 2006.

[6] G.E. Karniadakis and K.-S. Choi. Mechanisms on Transverse Motions in Turbulent Wall Flows. *Ann. Rev. Fluid Mech.*, 35:45–62, 2003.

[7] Y. Peet, Y. Sagaut, and P. Charron. Turbulent Drag Reduction using Sinusoidal Riblets with Triangular Cross-Section. In *38th AIAA Fluid Dynamics Conference and Exhibit*. Seattle, WA, June 2008.

[8] M. Quadrio. Streamwise-traveling waves of spanwise velocity at the wall of a turbulent channel flow. In *iTi Conference on Turbulence, Bertinoro (I), October 12-15, 2008*, 2008.

[9] M. Quadrio and P. Luchini. Method for reducing the friction between a fluid and an object. WO 2009/000703 A1.

[10] M. Quadrio, P. Ricco, and C. Viotti. Streamwise-traveling waves of spanwise wall velocity for turbulent drag reduction. *J. Fluid Mech.*, 627:161–178, 2009.

[11] M. Quadrio and S. Sibilla. Numerical simulation of turbulent flow in a pipe oscillating around its axis. *J. Fluid Mech.*, 424:217–241, 2000.

[12] M. Quadrio, C. Viotti, and P. Luchini. Skin-friction drag reduction via steady streamwise oscillations of spanwise velocity. In J.M.L.M. Palma and Silva Lopes A., editors, *Advances in Turbulence XI*, Advances in Turbulence XI, pages 659–661. Springer, 2007.

[13] P. Ricco and M. Quadrio. Wall-oscillation conditions for drag reduction in turbulent channel flow. *Int. J. Heat Fluid Flow*, 29:601–612, 2008.

[14] G. Schrauf. Key Aerodynamic Technologies for Aircraft Performance Improvement. In 5th Community Aeronautics Days, 2006.

[15] Tadmor. Line energy and the relation between advancing, receding, and Young contact angles. *Langmuir*, 20:7659–7664, 2004.

[16] H. Zhao, J.-Z. Wu, and J.-S. Luo. Turbulent drag reduction by traveling wave of flexible wall. *Fluid Dyn. Res.*, 34:175–198, 2004.